Lasers in Manufacturing Conference 2023

# Polarization-dependent bulk modification of $SiO_2$ by a femtosecond laser with pulse-front tilt

Qiang Fu[a,b], Cheng-Wei Wang[c,*], Hong-Jin Li[a], Quan-Zhong Zhao[a,b,1], Huai-Hai Pan[a], Jing Qian[a], Guan-De Wang[a], and Yu-Xing Zhao[c]

[a]*State Key Laboratory of High Field Laser Physics and CAS Center for Excellence in Ultra-intense Laser Science, Shanghai Institute of Optics and Fine Mechanics, Chinese Academy of Sciences, Shanghai 201800, China*
[b]*University of Chinese Academy of Sciences, Beijing 100049, China;*
[c]*Suzhou Delphi Laser Co., Ltd., Suzhou 215000, China*

**Abstract**

The polarization-dependent machining morphology in amorphous and monocrystalline $SiO_2$ machined by femtosecond laser is explained by second harmonic and tilted plasma due to PFT. While the polarization state changed from s-polarization to p-polarization, the machined region length of amorphous and monocrystalline $SiO_2$ increased by 25.1% and 97.9% separately, although the wave vector direction, the PFT sign, and the writing direction were the same. The plasma distribution under the irradiation of 182 fs laser pulse with PFT of 4.41 fs/mm is calculated by the plasma evolution model based on strong field and avalanche ionization. The tilted plasma leads to not only weaker reflection of p-polarized first harmonic than the s-polarized first harmonic, but also resonant absorption at the p-polarization state instead of s-polarization state. The integral of the reflected second harmonic at p-polarization was 56.5% of that at s-polarization for monocrystalline $SiO_2$ due to larger SHG coefficient at s-polarization.

Keywords: Femtosecond laser; pulse front tilt; plasma evolution

## 1. Introduction

Femtosecond lasers have been employed for fabricating waveguides, metal nanoparticles, nanogratings inside of transparent dielectrics because of their superior advantages (Qiu et al. 2004; Shimotsuma et al. 2003, 2005). However, the stability of machining morphology inside of materials is influenced by relatively high intensity and wide spectrum of femtosecond laser. Nonlinear effects prevents femtosecond pulses to induce

* Corresponding author: Quan-Zhong Zhao. Tel.: +86 021-69918749.
*E-mail address:* zqz@siom.ac.cn.

neat and elongated microstructures in 0.7 mm thick BK7 glass (Garzillo et al. 2016). Kerr self-focusing leads to the change of filament starting with polarization (Dharmadhikari et al. 2007), and possibly underlies the dependence of the machined morphology on the beam polarization. The change in the refractive index by Kerr self-focusing linearly depends on the nonlinear refractive index, which is related to the laser beam polarization (Adair, Chase, and Payne 1989).

The wide spectrum of femtosecond laser possibly results in angular dispersion, spatial and temporal chirp, which contributes to pulse-front tilt (PFT). The morphology of the dielectrics machined by femtosecond laser beams with PFT was affected by the wave vector direction, the PFT sign, and the writing direction, as well as by the direction of polarization. The dependence of machined microstructures on the wave vector direction were observed in $LiNbO_3$ crystals irradiated by a femtosecond laser beam with PFT (Yang, Kazansky, and Svirko 2008). The microstructures which were fabricated with a femtosecond laser beam depended on the PFT sign (Yang, Kazansky, Shimotsuma, et al. 2008). In addition, the machined region size of amorphous $SiO_2$ varied with writing direction (Vitek et al. 2010). When the writing direction was from the pulse tail to the pulse front, the machined area in amorphous $SiO_2$ was only slightly damaged and exhibited birefringence (Yang, Kazansky, Shimotsuma, et al. 2008). However, the machined area was heavily damaged when the writing direction was from the pulse front to the pulse tail. This phenomenon was explained by the tilted plasma that was ionized by the femtosecond laser beam with PFT (Bulgakova, Zhukov, and Meshcheryakov 2013).

In the present paper, the dependence of the machined region size on the laser beam polarization was measured in $SiO_2$ when the wave vector direction, the PFT sign, and the writing direction were fixed. When the polarization direction is perpendicular or parallel to the main plane composed by the propagation direction and the x direction, the laser beam is regarded as s-polarization or p-polarization respectively. Based on the direction of grating pair in the compressor of femtosecond laser, the PFT is in the main plane. The polarization-dependent machining morphology has been reported in the alumina silicate glass machined by a femtosecond laser beam with PFT. The length of the machined region was 27 μm in the p-polarization state, which was 12.5% larger than the value in the s-polarization state (Kazansky et al. 2011). The polarization-dependent machining morphology in amorphous and crystalline $SiO_2$ machined by femtosecond laser is probably caused by second harmonic and tilted plasma due to PFT. It was found that the plasma in amorphous $SiO_2$ irradiated by a femtosecond laser was tilted in the shadowgraph experiment due to PFT (Z. Wang et al. 2015).

## 2. Experiment

The experimental setup of laser machining, coaxial image system and reflection spectra measurement is shown in Fig. 1. The femtosecond laser beam from a 1 kHz Ti:sapphire laser (Spectra Physics Spitfire) was focused by a 10 times objective lenses with the numerical aperture (NA) of 0.30 into the $SiO_2$ samples. The front and side views of machined morphology were monitored by an optical microscope (Nikon Eclipse ME600) and photographed by a charge-coupled device (CCD). The $SiO_2$ samples were moved by a three-dimensional stage (Prior Scientific ProScan II) toward the objective lenses at the distance of $d_0$ = 200 μm after the upper surface of $SiO_2$ samples emerged on the CCD (Mshot MC-50) of the microscope. The distribution of laser intensity was Gaussian in space from the regenerative cavity and the laser diameter was 5.4 mm. The pulse energy $E_p$ was 25 μJ, which was measured by a power meter (Coherent PM3) after the objective lenses. And the pulse duration was 182 fs from an autocorrelator (APE mini). The CCD and coupled lens of the fibre spectrometer were lay at the image points, which were conjugated with the objective points at the focus. The reflective mirror R1 was insertable. The reflection spectra of monocrystalline and amorphous $SiO_2$, which were irradiated by the femtosecond laser, were recorded by a fibre spectrometer (Ocean Optics USB2000+) in Fig. 1. According to the reflection spectra, the central wavelength of femtosecond laser was 786 nm.

The objective lens, focus position, laser diameter, pulse energy, pulse duration and central wavelength were the same for both laser machining and spectra measurement experiments. The polarization of the femtosecond laser was adjusted by a half-wave plate (Thorlabs). The irradiation time of each exposure, which was controlled by a shutter (Thorlabs SH05), was fixed to 100 ms in the laser machining experiment for both polarizations.

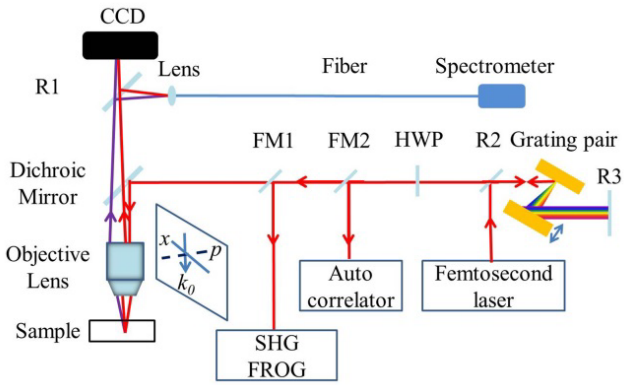


Fig. 1. Experimental setups of femtosecond laser machining, coaxial image system, reflection spectra and PFT measurements. FM1, FM2: flip mirrors. HWP: half-wave plate. R1, R2, R3: reflective mirrors. The wave vector $k_0$ and $x$ axis composes the main plane and the PFT $p$ is placed in the main plane

Apart from laser machining, coaxial image system and, reflection spectra measurement, the experimental setup includes PFT measurement in Fig. 1. The main plane, which is perpendicular to the paper, is illustrated. The direction of wave vector $k_0$ in Fig. 1 was normal to the C plane of monocrystalline $SiO_2$, which is in the same direction with the z axis. The compressor, which was composed by a pair of gratings on the right side of Fig. 1, was a part of the femtosecond laser. Because the grating vector was horizontal, the gratings in the compressor diffracted the laser beam in the horizontal plane. The pulse duration was detected by the autocorrelator and the PFT was measured by a FROG (Grenouille 8-20).

Six faces of both monocrystalline and amorphous $SiO_2$ were polished and used in the experiments. The monocrystalline $SiO_2$ sample (20 mm × 10 mm × 0.5 mm, Shanghai Daheng Optics and Fine Mechanics Co., Ltd.) was α-quartz, which belongs to crystal system 32. Two 20 mm × 10 mm faces were cut along the C plane (0001), and two 20 mm × 0.5 mm faces were cut along the M plane $(01\bar{1}0)$. Consequently, the 20-mm-length edge on the M plane was parallel to the crystal orientation [1000], which was the x axis in the system of crystal coordinates. Since the femtosecond laser propagated normally on the C plane of monocrystalline $SiO_2$, the polarization directions were always on the C plane. Furthermore, the polarization direction was parallel or perpendicular to the x axis when the polarization direction was parallel or perpendicular to the 20-mm-length edge, respectively. For comparison, amorphous $SiO_2$ (JGS1) with the size of 5 mm × 5 mm × 1 mm was used.

## 3. Results and discussion

This section is divided into the phenomenon of polarization-dependent machined morphology of the $SiO_2$ irradiated by the femtosecond laser with PFT and its explanation.

### *3.1. Polarization-dependent machined morphology of the $SiO_2$ irradiated by the femtosecond laser with PFT*

The machined morphology of both monocrystalline and amorphous $SiO_2$ varied with polarizations while the femtosecond laser propagated normally on the interface of air and $SiO_2$. The main plane is parallel to the face of paper in Fig. 2(a) and (c). And the wave vector $k_0$ and the $x$ axis are in the main plane. The laser beam was focused into the $SiO_2$ samples by the objective lenses with the focal length of $f$ = 20 mm.

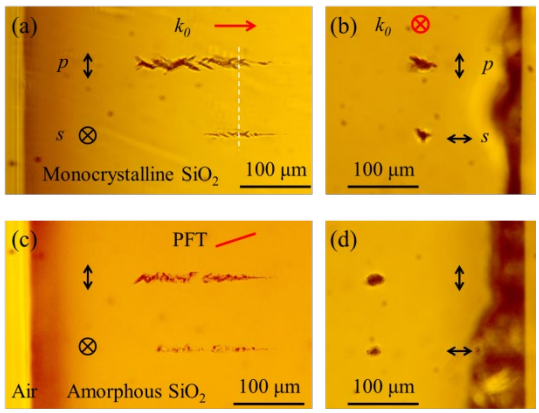


Fig. 2. The machined morphology of the $SiO_2$ samples which were irradiated by the femtosecond laser pulses with PFT in different polarization states. Machined morphology of monocrystalline $SiO_2$: (a) front view, (b) side view. Machined morphology of amorphous $SiO_2$: (c) front view, (d) side view. The white dashed lines in (a) indicate the positions of geometrical focus

The machined morphology of both monocrystalline and amorphous $SiO_2$ varied with polarizations, though the femtosecond laser propagated normally on the interface of air and $SiO_2$. As is illustrated in Fig. 2(a) and (c), the distances between the surface of monocrystalline and amorphous SiO2 and the starting of the machined region, which was induced by the s-polarized laser pulses, were 254 μm and 180 μm, and the machined region extended to 364 μm and 339 μm respectively. The length of machined region of monocrystalline and amorphous $SiO_2$ was 110 μm and 159 μm respectively in the s-polarization state. Thus the machined length of amorphous $SiO_2$ by s-polarized laser pulses was 44.7% longer than that of monocrystalline $SiO_2$. In contrast, the distances between the surface of monocrystalline and amorphous $SiO_2$ and the starting of the machined area, which was induced by the p-polarized laser beam, were 151 μm and 147 μm, respectively, and the machined region extended to 368 μm and 345 μm. The length of machined region of monocrystalline and amorphous $SiO_2$ was 217 μm and 198 μm in the p-polarization state respectively. Thus the machined length of amorphous $SiO_2$ by p-polarized laser pulses was 9.6% longer than that of monocrystalline $SiO_2$. As a consequence, the machined length of monocrystalline $SiO_2$ for machining with the p-polarized laser pulses was 97.9% larger than the length obtained by the s-polarized laser pulses. And the machined length of amorphous $SiO_2$ by p-polarized laser pulses was 25.1% larger than that by the s-polarized laser pulses.

The side view in Fig. 2(b) is more irregular than Fig. 2(d). This is probably caused by the structure difference of anisotropic monocrystalline and isotropic amorphous $SiO_2$. The crystal plane $\{10\bar{1}n\}$ (n is an integer) is more easily broken than other planes (Goltrant et al. 1992). The upper left crack at both p-polarization and s-polarization in Fig. 2(b) is approximately parallel to the $[1\bar{1}0n]$ plane which belongs to $\{10\bar{1}n\}$.

### *3.2. Explanation on the polarization-dependent machined morphology of $SiO_2$*

The polarization-dependent is probably caused by PFT instead of interface spherical aberration, Fresnel's reflection and Kerr self-focusing, because both the linear and nonlinear refractive index of $SiO_2$ in the s-polarization are the same with that in the p-polarization state.

3.2.1 Interpolating PFT Value of Femtosecond Laser

Although standard FROG measures spatial chirp instead of PFT. Grenouille adopted a biprism, rather than a common partial reflector, so as to split the same pulse from the centre (Akturk et al. 2003). The modified FROG is able to obtain the magnitude and sign of PFT (Akturk et al. 2003). For example, the PFT value was 6.82 fs/mm in Fig. 3 at the pulse duration of 155 fs.

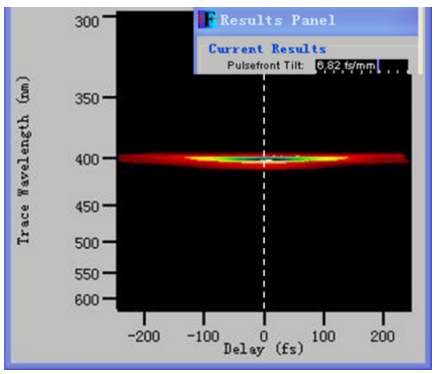


Fig. 3. Example of measured FROG trace

The PFT at different pulse duration was measured directly by the FROG. The PFT value for the pulse duration of $\tau_1$ =182 fs is interpolated and its value is $p_1$=4.41 fs/mm for the experiments of laser machining and reflection spectra. The PFT angle $\psi$ satisfies $\tan(\psi)=p_1 c$ (Akturk et al. 2004). Although the PFT angle before the objective lenses was only 0.0758°, the beam radius decreased after the beam passed through the objective lenses, and the PFT angle was increased significantly (Kazansky et al. 2011). The beam waist was $w_0=\lambda f/(n_0 \pi w_1)$=1.28 μm (C. Wang et al. 2015) in amorphous $SiO_2$. The PFT was $9.34\times10^3$ fs/mm at the beam waist and the PFT angle was as large as 70.3°. Apart from the value of PFT, direction of PFT could also be gained. Because the gratings in the compressor diffracted the laser beam in the horizontal plane, the angular dispersion is horizontal and the optical distance of wavelengths varied horizontally, for which GDD (group delay dispersion) is in the horizontal plane. The direction of both spatial chirp and PFT were in the horizontal plane. Therefore, the main plane was horizontal before the dichroic mirror and was turned 90° after the dichroic mirror in Fig. 1.

*3.2.2 Plasma evolution under the irradiation of the femtosecond laser with PFT*

To simulate the evolution of plasma produced by the front part of femtosecond laser pulse with PFT, the electric field and laser intensity in the time domain are calculated. Because the instantaneous laser intensity at the front part of femtosecond laser pulse is low, the nonlinear effects can be neglected. The laser beam propagated in the z direction and the laser electric field $E(z, x, \omega)$ in the frequency domain is as follows (Akturk et al. 2004):

$$E(z,x,\omega)=E_0(z)\exp\left[-\left(\frac{x}{w'}\right)^2\right]\exp\left[-\frac{(\tau')^2}{4}(\omega-\nu x)^2\right]\exp\left(-i\frac{\varphi^{(2)}}{2}\omega^2\right)\exp(-ik_0\beta\omega x) \quad (1)$$

where $\omega$, $w'$ and $v$ correspond to the circular frequency, the spot radius and the frequency gradient, respectively.

The electric field in the time domain is the inverse Fourier transform of the electric field in the frequency domain, namely $E(z, x, t)=1/(2\pi)*\int E(z, x, \omega)\exp(-i\omega t)\, d\omega$:

$$E(z,x,t)=\frac{E_0(z)}{\sqrt{\pi\left[(\tau')^2+2i\varphi^{(2)}\right]}}\exp\left[-\left(\frac{x}{w'}\right)^2-\frac{1}{4}x^2(\tau')^2\upsilon^2\right]\exp\left[-\frac{\left[2t+2k_0x\beta+ix(\tau')^2\upsilon\right]^2}{4\left[(\tau')^2+2i\varphi^{(2)}\right]}\right] \quad (2)$$

where $E_0(z)$ depends on the laser amplitude. The term $\{[\pi(\tau')^2+2i\varphi^{(2)}]\}^{-0.5}$ can be reduced to $A\exp(i\delta)$. The amplitude $A$ and the tangent argument tan $\delta$ are $\{[\pi^2(\tau')^4+4(\varphi^{(2)})^2]\}^{-0.25}$ and $-2\varphi^{(2)}/\{(\tau')^2+[(\tau')^4+4(\varphi^{(2)})^2]^{0.5}\}$, respectively. Due to the spatial chirp $\zeta$, the local spectral width decreased and the pulse duration parameter $\tau_0$ is increased to $\tau'$. It should be noted that the time term is nearly $\exp(-t^2/\tau_0^2)$ in Eq. (2), the parameter $\tau_0$ is equivalent to $\tau_1/(2\ln 2)^{0.5}$. The measured spatial chirp before the objective lenses was -29.1 fs·mm. The spot size obeyed the hyperbolic distribution. The $z$ coordinate at the focus was set to 0, so the waist radius $w(z)$ was equal to $w_0(1+z^2/z_0^2)^{0.5}$. The Rayleigh distance $z_0$ was equal to $k_0w_0^2/(2M^2)$ and the experimental $M^2$ factor was 1.33. The analytic expression for the $AE_0(z)$ was $E_{peak}*w_0/w(z)*\exp[ik_0x2/2R(z)]\exp[ik_0z-i\times\text{atan}(\lambda z/\pi w_0^2)]$ (C. Wang et al. 2015). The electric field at the focus $E_{peak}$ equals $(2I_0/\varepsilon_0cn_0)^{0.5}$ and the peak laser intensity $I_0$ is $4(\ln 2/\pi)^{0.5}E_p/(\pi w_0^2\tau_1)$ at the focus. The central wavelength $\lambda$ was 786 nm. The radius of curvature $R(z)$, which was caused by the focusing of the objective lenses, was $z(1+z_0^2/z^2)$. The electric field in the time domain is simplified as follows:

$$E(z,x,t)=E(z)\exp(i\delta)\exp\left[-\left(\frac{x}{w'}\right)^2\right]\exp\left[-\frac{(t+p_zx)}{\tau_m^2}\right]\exp\left\{-i\frac{\left[x\upsilon(\tau')^4-4k_0x\varphi^{(2)}\beta\right]\times t}{(\tau')^2+4(\varphi^{(2)})^2}\right\}$$

$$\times\exp\left[-i\frac{-2\varphi^{(2)}}{(\tau')^2+4(\varphi^{(2)})^2}\right]\exp\left[-i\frac{\left[\frac{(\tau')^4\varphi^{(2)}\upsilon^2}{2}+k_0\upsilon(\tau')^4\beta-2k_0^2\beta^2\varphi^{(2)}\right]x^2}{(\tau')^2+4(\varphi^{(2)})^2}\right]$$

$$E(z)=\frac{E_{peak}w_0}{w'}\exp\left(\frac{ik_0x^2}{2R(z)}\right)\exp\left\{-i\left[kz-\tan^{-1}\frac{\lambda z}{\pi\omega_0^2}\right]\right\}$$

$$\tau_m^2=(\tau')^2+\frac{4(\varphi^{(2)})^2}{(\tau')^2} \quad (3)$$

where the PFT $p_z$ is relative with the position $z$ and modified waist radius $w'(z)$ equals $(1/w(z)^2-v^2\tau_0^2/4)^{-0.5}$. The parameter $\tau_m$ was the pulse duration parameter modified by the GDD.

The time interval between the pulse front and pulse tail is unchanged even though the laser is focused by the objective lenses. Therefore, $p_z$ is approximate to $p_1*w_1/w'(z)$ after the lens. Because the pulse duration $\tau_1$ was 182 fs, the GDD $\varphi^{(2)}=\tau_p(\tau_1^2-\tau_p^2)^{0.5}/(4\ln 2)$ was $4.88\times10^3$ fs$^2$ . According to Eq. (3) and the relation between the intensity and the electric filed $I=0.5\varepsilon_0cn_0*E^2$, the laser intensity is expressed as follows:

$$I(z,x,t)=\frac{\varepsilon_0 c n_0 E_{peak}^2 w_0^2}{2(w')^2}\exp\left[-\frac{2x^2}{(w')^2}\right]\exp\left[-\frac{2(t+px)^2}{\tau_m^2}\right] \quad (4)$$

The polarization-dependent morphology of amorphous $SiO_2$ is influenced by PFT. The plasma density of amorphous $SiO_2$ is calculated in this paper, which is approximate to the plasma density of monocrystalline $SiO_2$. The free electron density $\rho$ evolves according to the following equation (Burakov et al. 2007):

$$\frac{\partial \rho}{\partial t}=w\times\frac{\rho_{VB}-\rho}{\rho_{VB}}+\times\frac{\sigma I}{E_g}\rho\times\frac{\rho_{VB}-\rho}{\rho_{VB}}-\frac{\rho}{\tau_r} \quad (5)$$

where the initial electron density in the $SiO_2$ valence band $\rho_{VB}$ is $3.2\times10^{29}$ $m^{-3}$. The strong field ionization rate $w$ is calculated by Keldysh formula directly (Keldysh 1965). The recombination time $\tau_r$ and the electron collision time $\tau_c$ in $SiO_2$ are 170 fs and 1.7 fs respectively (Sun et al. 2005), and the inverse Bremsstrahlung coefficient $\sigma$ equals $e^2\tau_c/(1+\omega^2\tau_c^2)/(\varepsilon_0 m_e c n_0)=7.1\times10^{-22}$ $m^2$ (Couairon and Mysyrowicz 2007). The energy gap $E_g$ is 9.43 eV (O' Brien et al. 1991).

Plasma density was obtained from Eq. (4) and Eq. (5). The integration time is from the lower limit $t_l$=-8$\tau_1$–($z$+3$L$/4)$n_0/c$ to the upper limit $t_u$=-2$\tau_1$–$zn_0/c$. And the simulation length $L$ in propagation direction is 360 μm, which is larger than the machined size in Fig. 2. The peak of the laser pulse on the $z$ axis moved from the starting $z_s$=-8$\tau_1 c/n_0$-3$L$/4=-570 μm to the ending $z_e$=-2$\tau_1 c/n_0$=-75 μm. For the zero point, the integration time is from -8$\tau_1$-3$Ln_0$/4$c$=-15$\tau_1$ to -2$\tau_1$, which is the front part of laser pulse.

The tilt of plasma is induced by PFT. As is shown in Fig. 4(a), the plasma does not incline when the PFT is 0. This is corresponding to the uninclined shadowgraph of plasma when the PFT is 0 (Z. Wang et al. 2015). The machined textures for two polarizations were nearly the same when the PFT was small (Kazansky et al. 2007). However, the plasma is tilted when PFT is significant in Fig. 4(b). The plasma, which is produced by the front part of femtosecond laser pulse, reflects the middle and latter parts of laser pulse. Therefore, the plasma density induced by the p-polarized laser is more than that by the s-polarized laser, which agrees with the shadowgraph at different polarizations (Z. Wang et al. 2015).

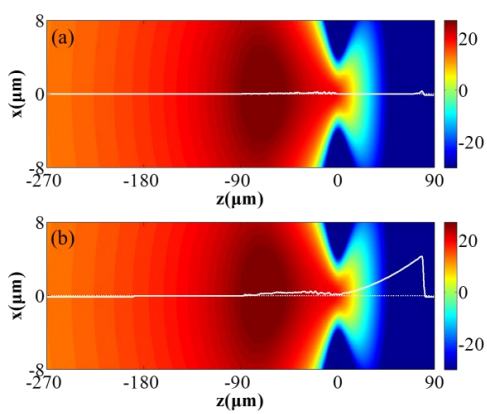


Fig. 4. Distribution of logarithmic plasma density at different PFT values: (a) p1=0, (b) p1=4.41 fs/mm. The white solid lines indicate the x coordinates of the maximum plasma density at any z coordinates and the white dotted lines are the propagation axis for reference

The reflectance of s-polarized laser by the tilted plasma is more than that of p-polarized laser and the resonant absorption enhances the laser intensity in the p-polarization state instead of s-polarization state. According to the white solid line in Fig. 4(b), the coordinates of two points are [$z$, $x$] = [-73 μm, 0.14 μm] and [-56 μm, 0.37 μm]. The plasma is tilted at the angle of $\vartheta_t$ = 0.78° near the ending point $z_e$ = -75 μm. The plasma density is obviously tilted behind the zero point, which is caused by the tilted pulse front, namely PFT. The plasma density in Fig. 4(b) reaches $\rho_z = 3.81\times10^{27}$ m$^{-3}$ at the position of [$z$, $x$] = [-81 μm, 0]. The relative dielectric function is reduced to $\varepsilon_r = n_0^2 - \rho_z e^2/(\varepsilon_0 m_e \omega^2) = 2.3\times10^{-3}$ and the refractive index is $n_p = \varepsilon_r^{0.5} = 0.048$ at the position of [$z$, $x$] = [-81 μm, 0]. In order to analyse the reflection and resonant absorption of laser by plasma, the gradient of plasma density is approximately parallel to the tangent line of the white solid curve in Fig. 4, namely the plasma density is constant in the plane normal to the plasma density gradient. The refractive angle in the plasma is $\vartheta_t^2 = \text{asin}(n_0/n_p \sin\vartheta_t) = 24°$ at the incident angle of $\vartheta_t$. The reflection at the interface of plasma and amorphous $SiO_2$ is $\sin^2(\vartheta_t-\vartheta_{t2})/\sin^2(\vartheta_t+\vartheta_{t2})$=89% and $\tan^2(\vartheta_t-\vartheta_{t2})/\tan^2(\vartheta_t+\vartheta_{t2})$ = 86% in the s-polarization and p-polarization state respectively (Liang 2008). Consequently the reflectance of the first harmonic by tilted plasma in the p-polarization state is less than that in the s-polarization state. The component of electric field along the plasma density gradient in the p-polarization state is equal to $\sin(\vartheta_t)E(z, x, t)$, while the component is 0 in the s-polarization state. Therefore, the component of electric field in the p-polarization state is improved to $\sin(\vartheta_t)E(z, x, t)/\varepsilon_r = 5.9E(z, x, t)$ (Kruer 2003). In other words, the laser intensity in the p-polarization state is increased significantly due to resonant absorption. The laser intensity of p-polarized laser is stronger than that of s-polarized laser due to resonant absorption. The high density plasma cuts down the dielectric function to nearly 0 and the inclination of plasma distinguishes s-polarization from p-polarization.

### *3.2.3 Polarization-Dependent Second-harmonic Generation of $SiO_2$*

The purpose of this section is to describe the influence of second harmonic generation (SHG) on the polarization-dependent modification of $SiO_2$. The spectra were plotted versus wavelength in Fig. 5 and each curve of reflected intensity was the average of 6 measured spectra. The directions of p-polarized and s-polarized laser were parallel and perpendicular to the crystal orientation [1000], namely the x axis of monocrystalline $SiO_2$, respectively, because the x axis of monocrystalline $SiO_2$ was put in the main plane.

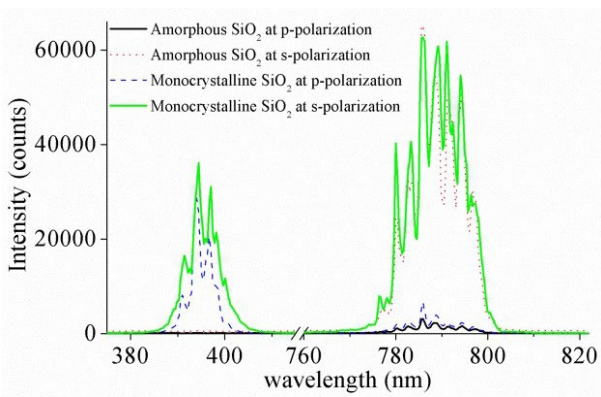


Fig. 5. Reflection spectra of monocrystalline and amorphous SiO2 which were irradiated by femtosecond laser with PFT in different polarization states

If the SHG is caused by plasma (Kruer 2003), there is SHG when amorphous $SiO_2$ is irradiated by femtosecond laser. However, SHG in amorphous $SiO_2$ is not detected in Fig. 5. That's maybe the reason why

the length of machined region in amorphous SiO2 at s-polarization or p-polarization is 44.7%, 9.6% longer than that in monocrystalline $SiO_2$ at s-polarization or p-polarization respectively.

The depletion of first harmonic due to SHG is mainly influenced by SHG coefficient. The effective coefficient $d_{eff}$ is expressed in the following equation when the laser irradiates on the C-plane of monocrystalline $SiO_2$,

$$d_{eff} = -d_{11}\sin(3\Phi), \quad o + o \to o \tag{6}$$

where $d_{11}$ is a tensor component of dielectric constant. $\Phi$ is the angle between $x$ axis and the face containing $z$ axis and wave vector. When the polarization direction is perpendicular to $x$ axis, $d_{eff}$ is equivalent to $d_{11}$, which is larger than the effective coefficient of second harmonic when the polarization direction is parallel to $x$ axis. This is the reason why the spectral integration of SHG in the p-polarization state is only 56.5% of that in the s-polarization state in Fig. 5.

## 4. Conclusions

In summary, the polarization-dependent bulk modification of amorphous $SiO_2$ is probably caused by tilted plasma induced by femtosecond laser with PFT. When the polarization direction is perpendicular or parallel to the main plane composed by the propagation direction and the x axis, the laser beam is regarded as s-polarization or p-polarization respectively. When the polarization state of the femtosecond laser beam changed from s-polarization to p-polarization, the machined region size of monocrystalline and amorphous $SiO_2$ increased by 97.9% and 25.1% respectively. The PFT value for the pulse duration of 182 fs was 4.41 fs/mm for the experiments of laser machining and reflection spectra. The distribution of plasma, which is developed by strong field ionization and avalanche ionization, is simulated in this paper and the plasma is tilted at the angle of 0.78° in the main plane. The tilted plasma leads to weaker reflection of first harmonic at p-polarization than s-reflection, and resonant absorption in the p-polarization instead of s-polarization state.

The tilted plasma is one reason why longer modification happens at p-polarization than s-polarization in monocrystalline $SiO_2$. Another reason is the polarization-dependent SHG. The directions of p-polarized and s-polarized laser beam were parallel and perpendicular to the crystal orientation [1000], namely the x axis, respectively, because the x axis of monocrystalline SiO2 was put in the main plane. The SHG coefficient when the polarization is parallel to x axis (p-polarization) is larger than that when the polarization is perpendicular to x axis (s-polarization). This is the reason why the spectral integration of SHG in the p-polarization state is only 56.5% of that in the s-polarization state in the reflection spectra. The depletion of first harmonic due to SHG at p-polarization is less than that at s-polarization for monocrystalline $SiO_2$.

## References

Adair, Robert, L. L. Chase, and Stephen a. Payne. 1989. “Nonlinear Refractive Index of Optical Crystals.” Physical Review B 39(5):3337–50.

Akturk, Selcuk, Xun Gu, Erik Zeek, and Rick Trebino. 2004. “Pulse-Front Tilt Caused by Spatial and Temporal Chirp.” Optics Express 12(19):4399–4410.

Akturk, Selcuk, Mark Kimmel, Patrick O’Shea, and Rick Trebino. 2003. “Measuring Pulse-Front Tilt in Ultrashort Pulses Using GRENOUILLE.” Optics Express 11(5):491–501.

Bulgakova, Nadezhda M., Vladimir P. Zhukov, and Yuri P. Meshcheryakov. 2013. “Theoretical Treatments of Ultrashort Pulse Laser Processing of Transparent Materials: Toward Understanding the Volume Nanograting Formation and ‘Quill’ Writing Effect.” Applied Physics B: Lasers and Optics 113(3):437–49.

Burakov, I. M., N. M. Bulgakova, R. Stoian, A. Mermillod-Blondin, E. Audouard, A. Rosenfeld, A. Husakou, and I. V. Hertel. 2007. “Spatial Distribution of Refractive Index Variations Induced in Bulk Fused Silica by Single Ultrashort and Short Laser Pulses.” Journal of Applied Physics 101(4):043506.

Couairon, A. and A. Mysyrowicz. 2007. “Femtosecond Filamentation in Transparent Media.” Physics Reports 441(2–4):47–189.

Dharmadhikari, A., K. Alti, J. Dharmadhikari, and D. Mathur. 2007. “Control of the Onset of Filamentation in Condensed Media.” Physical Review A 76(3):033811.

Garzillo, Valerio, Vytautas Jukna, Arnaud Couairon, Robertas Grigutis, Paolo Di Trapani, and Ottavia Jedrkiewicz. 2016. “Optimization of Laser Energy Deposition for Single-Shot High Aspect-Ratio Microstructuring of Thick BK7 Glass.” Journal of Applied Physics 120(1).

Goltrant, Olivier, Hugues Leroux, Jean-claude Doukhan, and Patrick Cordier. 1992. “Formation Mechanisms of Planar Deformation Features in Naturally Shocked Quartz.” Physics of the Earth and Planetary Interiors 74:219–40.

Kazansky, Peter G., Yasuhiko Shimotsuma, Masaaki Sakakura, Martynas Beresna, Mindaugas Gecevičius, Yuri Svirko, Selcuk Akturk, Jianrong Qiu, Kiyotaka Miura, and Kazuyuki Hirao. 2011. “Photosensitivity Control of an Isotropic Medium through Polarization of Light Pulses with Tilted Intensity Front.” Optics Express 19(21):20657–64.

Kazansky, Peter G., Weijia Yang, Erica Bricchi, James Bovatsek, Alan Arai, Yasuhiko Shimotsuma, Kiyotaka Miura, and Kazuyuki Hirao. 2007. “‘Quill’ Writing with Ultrashort Light Pulses in Transparent Materials.” Applied Physics Letters 90(15):151120.

Keldysh, L. V. 1965. “Ionization in the Field of a Strong Electromagnetic Wave.” Soviet Physics JETP 20(5):1307–14.

Kruer, William L. 2003. The Physics of Laser Plasma Interactions. Colorado: Westview Press.

Liang, Quanting. 2008. Physical Optics. Beijing: Publishing house of electronics industry.

O’Brien, W. L., J. Jia, Q. Y. Dong, T. A. Callcott, J. E. Rubensson, D. L. Mueller, and D. L. Ederer. 1991. “Intermediate Coupling in L2-L3 Core Excitons of MgO, Al2O3, and SiO2.” Physical Review B 44(3):1013–18.

Qiu, Jianrong, Xiongwei Jiang, Congshan Zhu, Mitsuru Shirai, Jinhai Si, Nan Jiang, and Kazuyuki Hirao. 2004. “Manipulation of Gold Nanoparticles inside Transparent Materials.” Angewandte Chemie (International Ed. in English) 43(17):2230–34.

Shimotsuma, Yasuhiko, Kazuyuki Hirao, Peter G. Kazansky, and Jiarong Qiu. 2005. “Three-Dimensional Micro- and Nano-Fabrication in Transparent Materials by Femtosecond Laser.” Japanese Journal of Applied Physics 44(7A):4735–48.

Shimotsuma, Yasuhiko, Peter G. Kazansky, Jiarong Qiu, and Kazuoki Hirao. 2003. “Self-Organized Nanogratings in Glass Irradiated by Ultrashort Light Pulses.” Physical Review Letters 91(24):247405.

Sun, Quan, Hongbing Jiang, Yi Liu, Zhaoxin Wu, Hong Yang, and Qihuang Gong. 2005. “Measurement of the Collision Time of Dense Electronic Plasma Induced by a Femtosecond Laser in Fused Silica.” Optics Letters 30(3):320–22.

Vitek, Dawn N., Erica Block, Yves Bellouard, Daniel E. Adams, Sterling Backus, David Kleinfeld, Charles G. Durfee, and Jeffrey a Squier. 2010. “Spatio-Temporally Focused Femtosecond Laser Pulses for Nonreciprocal Writing in Optically Transparent Materials.” Optics Express 18(24):24673–78.

Wang, Chengwei, Quanzhong Zhao, Jing Qian, Yangbo Li, Guande Wang, Yang Zhang, Huaihai Pan, Zongjie Bao, Feng Bai, and Wenzhong Fan. 2015. “Propagation of Focused Ultrashort Pulse Laser during Micromachining of Sapphire.” P. 95320O in Proc. of SPIE. Vol. 9532, edited by J. Shao, T. Jitsuno, W. Rudolph, and M. Zhu.

Wang, Zhaohui, Bin Zeng, Guihua Li, Hongqiang Xie, Wei Chu, Fei He, Yang Liao, Weiwei Liu, Hui Gao, and Ya Cheng. 2015. “Time-Resolved Shadowgraphs of Transient Plasma Induced by Spatiotemporally Focused Femtosecond Laser Pulses in Fused Silica Glass.” Optics Letters 40(24):5726–29.

Yang, Weijia, Peter G. Kazansky, Yasuhiko Shimotsuma, Masaaki Sakakura, Kiyotaka Miura, and Kazuyuki Hirao. 2008. “Ultrashort-Pulse Laser Calligraphy.” Applied Physics Letters 93(17):171109.

Yang, Weijia, Peter G. Kazansky, and Yuri P. Svirko. 2008. “Non-Reciprocal Ultrafast Laser Writing.” Nature Photonics 2(2):99–104.